New insights from fractional order skyhook damping control for railway vehicles

Article *in* Vehicle System Dynamics · February 2018

DOI: 10.1080/00423114.2018.1435889

2 authors:

Argyrios Zolotas
University of Lincoln
109 PUBLICATIONS **799** CITATIONS
SEE PROFILE

Roger M. Goodall
Loughborough University
287 PUBLICATIONS **2,749** CITATIONS
SEE PROFILE

To appear in *Vehicle System Dynamics*
Vol. 00, No. 00, Month 20XX, 1–23

RESEARCH ARTICLE (P R E – P R I N T)

New insights from fractional order skyhook damping control for railway vehicles

A. C. Zolotas[a*] and R. M. Goodall[b]

[a]*School of Engineering, College of Science, University of Lincoln, Lincoln, LN6 7TS, UK;*
[b]*School of Mechanical, Electrical and Manufacturing Engineering, Loughborough University, Loughborough, Leicestershire LEI1 3TU, UK*

(*v1.02*)

Active suspensions for railway vehicles have been a topic of research for a number of decades and while their applications in service operation are limited it seems clear that they will in due course see widespread adoption. Railway suspension design is a problem of compromise on the non-trivial trade-off of ride quality vs track following (guidance), and the skyhook damping control approach has been paramount in illustrating the potential benefits. Since skyhook damping control, various advanced control studies appeared contributing to redefine the boundaries of the aforementioned trade-off. Yet there is no study on the impact of fractional order methods in the context of skyhook railway active suspensions, and in particular related to skyhook damping control. This is the area to which this paper strongly contributes.

We present findings from a current project on fractional order controllers for railway vehicles active suspensions, in particular work on the effect of fractional order methods in basic skyhook damping control schemes, i.e. pure and intuitively-based skyhook. Firstly we present a brief review of conventional skyhook damping control and then proceed to a rigorous investigation of the impact of fractional order on the ride quality / track following trade-off. The relevant benefits from fractional order methods are appraised and new insights highlighted.

Keywords: railway suspension; suspension control; ride comfort; fractional-order control; active suspension; fractional skyhook damping

1. Introduction

Active suspensions for railway vehicles have been under consideration now for a number of decades [1], although their applications in service operation are very limited [2]. Nevertheless it seems clear that they will in due course see widespread adoption, and for this reason on-going research studies are very appropriate. Control can be applied either to improve the performance of the secondary suspension (carbody to bogie), generally to give improved ride quality, or to the primary suspension (bogie to wheelsets), and can in principle operate in any direction (lateral, vertical, roll, etc.).

This study is focussed upon solutions for secondary suspensions, for which the concept

*Corresponding author. Email: azolotas@lincoln.ac.uk

of *absolute* or *Skyhook* damping is well known [3]. This gives a profound improvement to the ride quality for straight track operation, but creates large suspension deflections in response to long wavelength, deterministic features such as curves and gradients, [4], a characteristic that is not usually a significant design issue for passive suspensions using conventional dampers. Although this can be accommodated in the control design, e.g. by filtering out the low frequency components from the measurements which are largely caused by track deterministic features [4], it is recognised that reducing the deterministic deflections to an acceptable level will compromise the performance achievable with "pure" skyhook damping. In fact the absolute velocity signal that is required for skyhook damping will usually be produced by integrating the signal from an accelerometer, and so in practice it will also be necessary to filter out the low frequency components in order to avoid problems with thermal drift in the accelerometer.

Fractional order control has gained, especially recently, popularity in the control literature [5] and increasingly makes its way into industrial control applications such as in the process control industry, electrical machines, robotics [6] [7] [8] [9] [10]. Fractional control study growth is also seen in the automotive area albeit at a much slower rate. In particular, [11] discussed fractional PID control for nonlinear vehicle suspensions via evolutionary design methods, [12] presented a numerical scheme to design single fractional order derivative skyhook damping controllers to deal with nonlinearities in the suspensions on a quarter car vehicle (mainly touching ride comfort). Work in [13] presented FOPID design for a nonlinear suspension model with electro-hydraulic actuation, while [14] and [15] presented active suspension control design that mainly illustrated capabilities of the CRONE controller approach. There are resources dealing with semi-active related fractional order control, i.e. for active passenger seat control design [16], for a semi-active suspension [17], as well as smart-based isolated structures [18]. Not addressing skyhook control principles, the nature of the aforementioned material is very different to the work presented in this paper. A recent survey on conventional active and semi-active control can be seen in [19].

From a historical perspective, fractional order calculus (the concept on which fractional order control is based) dates back to the 17th century with a letter sent by L'Hôpital to Leibniz on the topic of derivatives. This excited replies between the two men on the concept of 'non-integer' order differentiation and/or integration. In particular, Leibniz raised the following question to L'Hôpital: "Can the meaning of derivatives with integer order be generalized to derivatives with non-integer orders?". L'Hôpital's was rather curious about it and his reply to Leibniz was a counter question, i.e. "What if the order will be 1/2?". In fact Leibniz, in a letter dated September 30th, 1695 essentially marks the date considered the exact birthday of fractional calculus when he replied: "It will lead to a paradox, from which one day useful consequences will be drawn" [20]. The work presented in this paper falls exactly within the remit of Leibniz's statement.

In the area of railway control applications (and especially those of a suspension design nature) fractional control is still in its infancy. A rather substantial set of benefits from using fractional order methods in the design of active tilt railway suspensions was recently presented in seminal work in [21], [22]. These two papers and work presented in [4], which forms a comprehensive study of conventional skyhook damping control achievement in railway suspensions, motivated the work presented in this paper. In fact, to the best of the authors' knowledge, there is yet to appear a rigorous study on the impact of fractional order methods in the context of skyhook damping control related railway active suspensions. This is the area to which this paper strongly contributes. We present fractional order design considerations within the remit of skyhook damping control for the suspension deflection vs ride quality improvement trade-off.

The paper is organised as follows: Section 2 presents a description summary of the skyhook schemes listed in the paper. Section 3 introduces the vehicle model including an insight into railtrack characteristics. Section 4 revisits basic (/practical) conventional skyhook damping control schemes [4] and presents the related achievements in terms of the ride quality and maximum suspension deflection trade-off including some optimization related enhancement. Section 5 presents a brief intro to fractional calculus and control, while Section 6 (lists the major contribution) rigorously discusses fractional order skyhook (basic/practical) control schemes. Some basic robustness insights are offered in Section 7, whereas conclusions and a list of the beneficial insights by use of fraction skyhook schemes are drawn in Section 8.

2. Skyhook control cases listed in the paper

Table 1 lists the various cases (conventional and fractional) that are used for comparative assessment in the following sections.

Table 1. Skyhook schemes listed in the paper

Type	**Abbrev.**	**Description**
Conventional integer forms	*Passive*	Passive suspension setup (incl. damping)
	pCsky (orig.)	Basic skyhook
	pCsky (mod.)	Basic skyhook (for max susp defl $\leq$ 60mm)
	iCsky(man.)*	Practical skyhook (manually designed; varying: high-pass filter (HPF) cut-off freq., while HPF damping ratio = 0.707)
	iCsky (optim.-A)*	Practical skyhook (optimised; varying: HPF cut-off freq., controller gain, and HPF damping ratio = 0.707)
	iCsky (optim.-B)*	Practical skyhook (optimised; varying: HPF cut-off freq., HPF damping ratio, controller gain)
Fractional order forms	*tpCsky*	Basic skyhook with only fractional-order integrator (optimised; varying: controller gain)
	*tiCsky**	Practical skyhook with fractional-order integrator and integer-order HPF (optimised; varying: HPF cut-off freq., HPF damping ratio, fractional integration order)
	*tifCsky**	Practical skyhook with fractional-order self-zero integrator (optimised; varying: the self-zero integrator's cut-off freq., its damping ratio, and its fractional integration order)

* The high-pass filter is of 2nd order;
"Optimised": Constrained optimization on minimizing ride quality subject to maintaining a 60mm max suspension deflection bound.

3. Modeling and track profile characteristics

3.1. *Vehicle model*

A quarter-car model, typical representation of secondary suspension setup in railway vehicles, is employed in this work for simplicity and ease of navigating through the new insights via fractional order methods in skyhook control schemes. However the proposed designs are applicable to more complex vehicle model classes (i.e. easily extendible to sideview vehicle model etc.). The passive suspension quarter-car model is seen in Figure 1(a), where a damper end-stiffness is also included. The values chosen are typical for high-speed trains nowadays and we opt to utilise the same set as the one used in [4] for a fairer comparison between conventional control schemes (and the related achievements shown in that paper) and the fractional-order approaches presented here. The parameters are: vehicle body mass $m = 30$ tonnes, secondary suspension stiffness $k_s = 700$ kN/m, secondary suspension damper end-stiffness $k_d = 7$ MN/m, and secondary suspension damper $c_s = 50$ kNs/m. A maximum suspension deflection limit of 60 mm is used in this work. The passive system setup with the aforementioned values results in a ride quality level of $\approx 3.37\%$g and maximum suspension deflection of 33.8mm.

3.2. *Rail track profiles*

As explained, the design trade-off is between the response to deterministic and random track inputs. This sub-section quantifies inputs drawn from typical railway applications practice.

For the deterministic input, a typical railway gradient of 1% is assumed with a superimposed acceleration limit of 0.5 m/s^2 (i.e. 5% g), a value that is specified for passenger comfort reasons and is used to determine the design alignment of the track. At a typical top speed of 55 m/s this corresponds to an 1.1 sec transitional section (it is noted that 55 m/s is the train speed used throughout this work).

Random inputs represent the misalignment of the track compared with the intended (deterministic) alignment, and these can be approximated by a power spectrum for the track position given by $A_\mathrm{r}/f_\mathrm{t}^2$ (m^2/(cyclem^{-1})), in which f_r is a spatial frequency (then converted to a temporal frequency via use of the train forward speed). A_r is a track roughness factor, commonly given a value of 2.5×10^{-7} for typical quality mainline track [23].

The results will depend upon the track characteristics that are used, and usually is necessary to recalculate as appropriate. In particular a route with less significant vertical gradients would enable a greater benefit in terms of ride quality. This paper nevertheless identifies the basic principles by which the trade-off can be determined.

4. Conventional skyhook damping control schemes

Seminal work in [4] has presented a rigorous study on the performance of linear and nonlinear conventional skyhook damping schemes (studied pure skyhook, intuitive skyhook implementation, complementary filter and Kalman Filter approaches). That specific study illustrated that the linear complementary filter scheme provided about 23% improvement in ride quality while maintaining a similar maximum suspension deflection level as the one provided by the original passive suspension. In addition, the specific non-linear Kalman filter methods provided nearly 50% ride quality improvement at the

expense of larger maximum suspension deflection compared to the passive case. The interested reader is referred to [4] for details in the aforementioned design aspects.

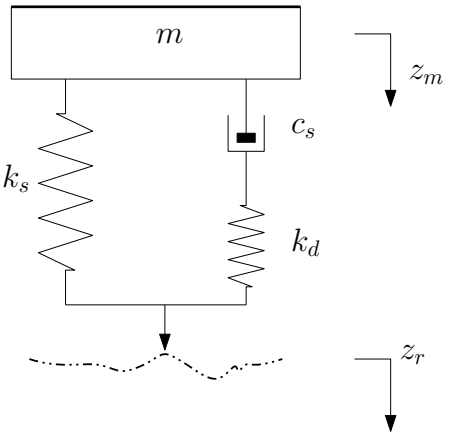

(a) Passive setup (with damper end-stiffness)

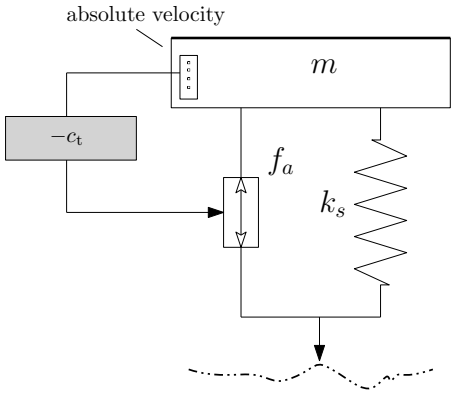

(b) Basic concept (conv. skyhook)

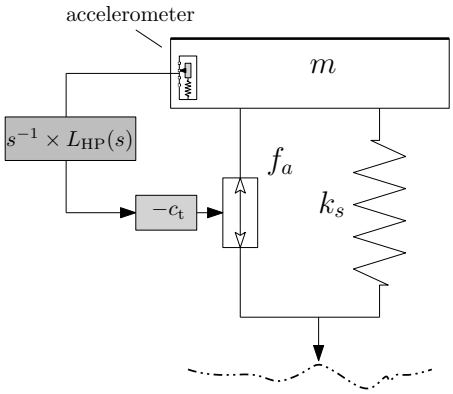

(c) Practical (self-zero integrator) skyhook implementation

Figure 1. Passive and skyhook damping control schemes

Here, we briefly revisit pure (basic) and intuitively (practical) implemented skyhook damping designs with these serving as baseline cases prior to introducing the (non-conventional) fractional order skyhook damping approaches. Figure 1(b) and Figure 1(c) present the conventional basic and self-zero integrator (practical or sometimes referred to as intuitively-based) skyhook damping control schemes, see [4]. The basic skyhook concept is based on the assumption that the vehicle body vertical velocity can be measured, albeit normally this is obtained from an accelerometer via so-called "self-zero" integration (i.e. a combined integrator and high-pass filter). The system's damping is introduced by the active element (actuator). Note that we refer to the practical conventional skyhook implementation as *iCsky*, while the pure conventional skyhook is referred to as *pCsky*.

"Conventional" in this context means the use of integer-order integration of the measured body acceleration signal. The controller gain is c_t, and also an ideal force actuator is assumed for this study.

4.1. *Basic (pure) skyhook damping control*

The system's equation of motion for pure skyhook damping, i.e. active force $f_a(t) = -c_t\dot{z}_m(t)$, is given by ($(t)$ dropped for simplicity)

$$m\ddot{z}_m + c_t\dot{z}_m + k_s(z_m - z_r) = 0 \tag{1}$$

whereby the damping contribution of "skyhook" is seen in $c_t\dot{z}_m$. Normally the (designed) vehicle systems's damping level is chosen to be around 65% to 70% [24], [25] (which dictates the relevant skyhook damping value in the pure skyhook damping control scheme.). Here, a value of $c_t = 190$ kNs/m results in 66% damping.

Given the aforementioned values, *pCsky* (man.) provides ride quality level of 1.1%g (based on single-sided spectrum) and a maximum suspension deflection of 156mm (see Figure 4, which also includes the passive suspension response and the modified basic skyhook damping scheme that adheres to 60mm maximum suspension deflection). The unacceptable suspension deflection level can be clearly seen, as well as the effect of skyhook damping on steady-state given the characteristics of the rail track profile used.

For completeness we also present the controller gain value which adheres to the limit of 60 mm maximum suspension deflection, i.e. $c_{t_{60}} = 51.1$ kNs/m (this gain results in 2.12%g ride quality and 17.7% minimum closed-loop damping), i.e. scheme *pCsky* (mod.). A summary of relevant performance results is listed on Table 2.

4.2. *Practical skyhook damping control*

Figure 2 presents the feedback setup[1] for *iCsky*. $G(s)$ is the design transfer function, i.e. actuator force input to measured body acceleration output, given by

$$G(s) = \frac{\ddot{z}_m}{f_a}(s) = \frac{s^2}{ms^2 + k_s} \tag{2}$$

It is worth noting that for conventional skyhook damping $L_i(s) := s^{-1}$ and $L_{HP}(s)$ is of integer order (also $\dot{z}^*_{\rm m} := \dot{z}_{\rm m}$), while for fractional order skyhook damping $L_i(s) = s^{(-1/n)}$ (the so called "tilted" integrator)[2]. Note that $\dot{z}^*_{\rm m}$, in the latter case is essentially a fractional body velocity element. Just for purpose of notation (distinguishing between conventional and fractional), the forward path controller gain is shown as $K_{\rm t}$ but we refer to this as $c_{\rm t}$ (for integer order skyhook damping schemes) or $k_{\rm t}$ (for fractional order skyhook damping). Tuning the controller gain will be further explained in the optimization studies.

As mentioned previously, absolute vertical velocity of the body is a difficult signal to be measured directly and it is obtained by the body's measured vertical acceleration filtered through "self-zero' integrator (i.e. an integrator combined with a high-pass filter). This attempts to provide a solution to both the integrator drift issue and to reducing the large, low-frequency deflections. In fact, work in [4] presented 1st, 2nd and 3rd order high-pass filters (HPF) with Butterworth response (with the latter two cases providing similar performance results in that study). The design here actually involves a 2nd integer-order

[1]Similar feedback structure is used for both the integer order skyhook and fractional order skyhook schemes for simplicity in diagram presentations. Note that the feedback setup is in the form of virtual "pure" skyhook damping (or actual "pure" skyhook damping if both $L_{\rm i}(s), L_{\rm HP}(s)$ are unity).

[2]The HP filter can be either of integer- or of fractional-order, or an overall fractional "self-zero" integrator can be followed.

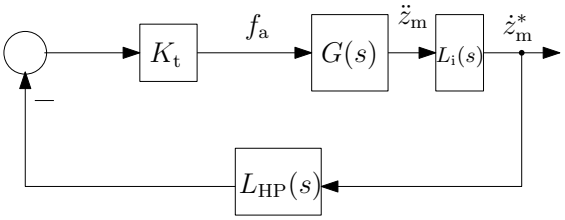

Figure 2. Feedback setup for implemented skyhook scheme

HPF (to avoid unnecessary increase in conventional controller order), see (A1), while $c_\mathrm{t} = 190000$ Ns/m. The closed-loop transfer function, from Figure 2, for *iCsky* is

$$T_{iCsky}(s) = \frac{G(s)K_\mathrm{t}}{s + L_{HP}(s)G(s)K_\mathrm{t}} \tag{3}$$

In addition, high-pass filter's frequency cut-off range that maintains closed-loop (absolute) stability is investigated via the Routh-Hurwitz test (see Appendix A), i.e.

$$\omega_\mathrm{fc} \in \left(0, \frac{-c_\mathrm{t} + \sqrt{c_\mathrm{t}^2 + 16\,k_\mathrm{s}\,m\,\xi^2}}{4\,m\,\xi}\right) \quad \text{(in rad/s)} \tag{4}$$

Substituting for the parameter values used in this work, $\omega_\mathrm{fc} \in (0, 0.95\pi)$ rad/s. Note that $K_\mathrm{t} := c_\mathrm{t}$ because of the conventional scheme studied here.

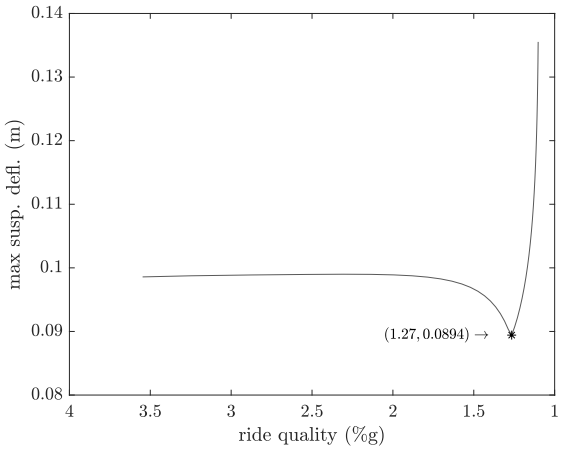

Figure 3. Deterministic/ Stochastic trade-off for iCsky (man.) (2nd order L_{HP})

With the aforementioned conditions for the filter cut-off frequency, a rather straightforward search is followed and results for the performance trade-off are obtained. The trade-off curve (varying the HPF's cut-off frequency ω_fc) is shown on Figure 3, including the point of minimum peak suspension deflection achieved (and accompanying ride quality value). Still the maximum suspension deflection level is unacceptable (and the only way to adhere to the 60mm max suspension limit is via gain variation as well). A summary of the performance results can be seen in Table 3 (which also lists the sensitivity peak of the designed closed-loop to overall changes in the plant transfer function, i.e. $\|S^p_{cl}(j\omega)\|_\infty$, which is inversely proportional to robustness and hence used as a basic robustness index [26]). In fact, the results agree with the discussion in the earlier paper

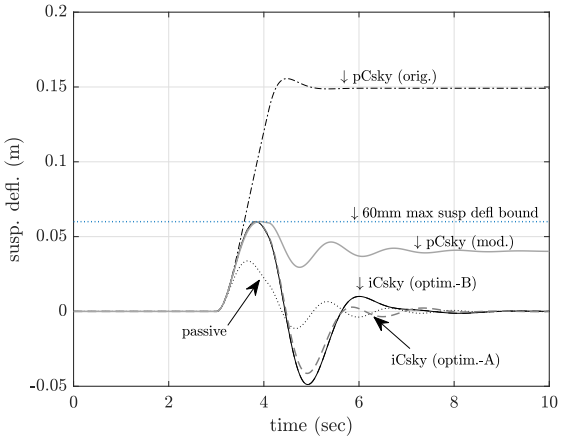

Figure 4. Suspension deflection conventional skyhook damping schemes (deterministic)

of Li and Goodall [4]For completeness, the deterministic suspension deflection response is shown on Figure 4.

Table 2. Basic skyhook damping control schemes performance result

Scheme	**Filter**	ride qual. (%g)†	max susp. delf. (mm)	min$\{\zeta\}$ (%)	$\|\mathbf{S_{cl}^{p}}(\mathbf{j}\omega)\|_\infty$ (abs)
Passive	-	3.37	33.8	17.3	
pCsky$^{(man.)}$	-	1.10	156.0	66.0	1.00
pCsky$^{(mod.)}$ *	-	2.12	60.0	17.7	1.00
tpCsky$^{(optim.)}$ *	-	2.11	60.0	16.7	1.02

† Single-sided spectrum; * Tuning of controller gain k_{t}.

4.3. *Optimised practical skyhook damping control*

To impose the 60mm maximum suspension deflection limit while minimising the ride quality level, the controller gain needs to be varied. Here we present two optimized versions of *iCsky*, i.e. *optim.-A* and *optim.-B* (see Table 1). This is also performed to enable appropriate comparison to the relevant fractional order schemes presented later on. Hence, the formulated optimization problem[3] is

$$\begin{aligned} \underset{\omega_{\mathrm{fc}},\omega_{\mathrm{ig}},\xi}{\text{minimize}} \quad & \text{ride quality (active conv.)} \\ \text{s. t.} \quad & \max\{|z_r - z_m|\} \leq 60\text{mm} \end{aligned} \tag{5}$$

[3]An extra constraint on the system's minimum closed-loop damping can be added, however it was not necessary as the obtained damping level was acceptable.

Remark. The variables used for the optimization process are: ω_{fc} and ξ which are the HPF cut-off frequency and damping ratio (this variable is varied in *iCsky* (optim.-B)), while ω_{ig} is the integrator gain crossover frequency (i.e. $\frac{\omega_{\text{ig}}}{s}$). The latter variable is selected, when controller gains is required to be also tuned, as an indirect way of tuning the gain. Hence, all optimization variables are maintained at comparable magnitude orders. The potential impact that the damping ratio of the 2nd order high-pass filter will have on the system performance is acknowledged, however in this study -and for all optimised schemes - we constrain its value to be no less than 0.55 (typically, for a 2nd order HPF, its value will be chosen ≈ 0.707 i.e. the Butterworth response mentioned in [4], [25]).

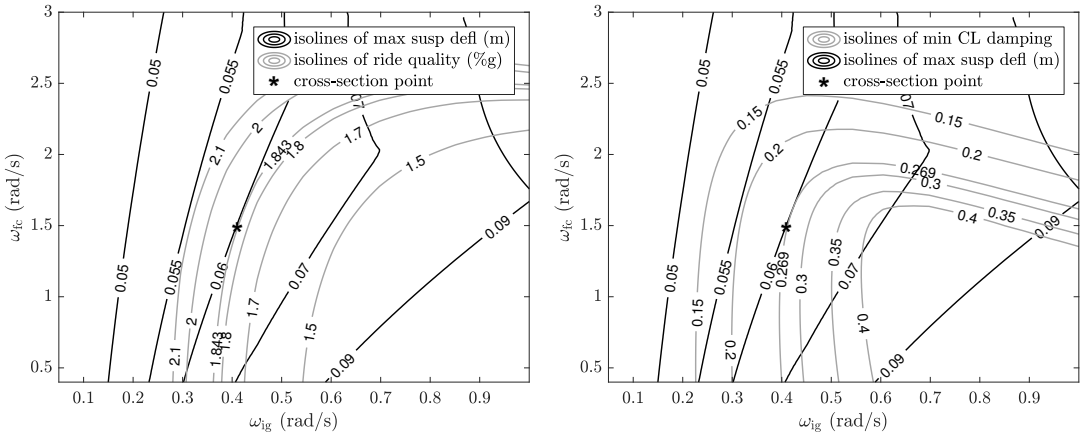

(a) Max susp defl and ride quality (*iCsky-A*)

(b) Max susp defl and min CL damping (*iCsky-A*)

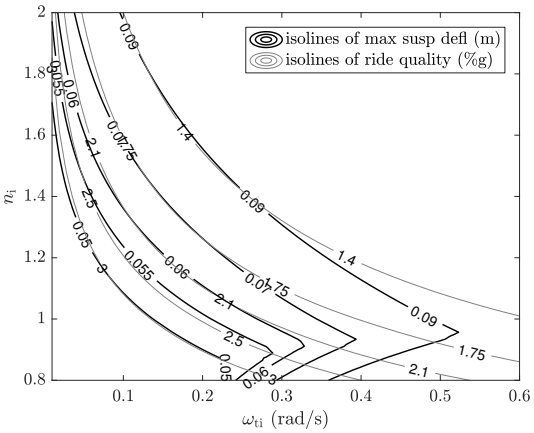

(c) Max susp defl and ride quality (*tpCsky*)

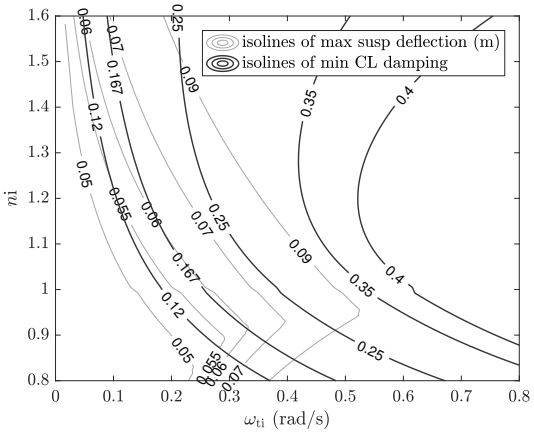

(d) Max susp defl and min CL damping (*tpCsky*)

Figure 5. Contour lines for optimised *iCsky* (optim.-A) and optimised *tpCsky*

For case *iCsky* (optim.-A) (recall that $\xi = 0.707$ here) the optimised parameters are[4].

$$\omega_{\text{fc}}^{opt} = 1.59 \text{ rad/s}, \;\; c_{\text{t}}^{opt} := \bar{c}_{\text{t}} \times \omega_{\text{ig}}^{\text{opt}} = 190\text{e}3 \times 0.419 = 79610 \text{ N/m} \tag{6}$$

The obtained minimum closed-loop damping was 26.9%. In fact, the point values can be visualised approximately on the intersection of the two isolines, i.e. of 60mm maximum susp deflection and ≈ 0.269 min CL damping level, as well as 60mm maximum susp deflection and ride quality level of ≈ 1.843%g (see Figures 5(a), 5(b)).

For case *iCsky* (optim.-B) the optimised parameters are:

$$\omega_{\text{fc}}^{opt} = 1.87 \text{ rad/s}, \;\; c_{\text{t}}^{opt} := \bar{c}_{\text{t}} \times \omega_{\text{ig}}^{\text{opt}} = 190\text{e}3 \times 0.417 = 79230 \text{ N/m}, \;\; \xi^{\text{opt}} = 0.55 \tag{7}$$

We do not present contour plots for the latter scheme as the concept is very similar. Also, Figure 4 presents the suspension deflection time-domain response for the deterministic track under identifiers *iCsky* (opt.-A), *iCsky* (opt.-B). The performance results for the schemes can be seen on Table 3 that summarizes the practical skyhook damping related approaches. It is worth noting that reducing HPF damping ratio value (i.e. lesser than a typical Butterworth response level [4]) contributes to improving ride quality (while worsening, as expected, sensitivity peak).

5. A brief introduction to fractional calculus and control

Fractional order integration/differentiation relates to the concept of 'non-integer' order, i.e. a more generalized version of integration/ differentiation. In fact, various definitions for the general fractional differential/integral exist [27] (e.g. by Riemann-Liouville, by Caputo etc.), with Caputo's approach offering the advantage of relating fractional order to physical realization.Caputo's fractional derivative is given by

$${}_aD_t^x f(t) = \frac{1}{\Gamma(n-x)} \int_a^t \frac{f^{(n)}(\tau)}{(t-\tau)^{x-n+1}} d\tau, \tag{8}$$

where $(n-1 < x < n)$; $\Gamma(.)$ the *Gamma function* and a, t the limits of operation of ${}_aD_t^x f(t)$. In addition its Laplace transform (with non-zero initial condition) is [27]

$$\int_0^\infty e^{-st} \left\{ {}_0D_t^x f(t) \right\} dt = s^x F(s) - \sum_{k=0}^{(n-1)} s^{x-k-1} f^{(k)}(0), \tag{9}$$

where $F(s) = \mathcal{L}\{f(t)\}$, $(n-1 < x \leq n)$ and s is the Laplace operator. Note that in the case of zero initial conditions (9) reduces to $\mathcal{L}\left\{ {}_0D_t^x f(t) \right\} = s^x F(s)$ (with $x < 0$ then the case of fractional integral of order $-x$ is also handled). Fractional order calculus tends to enable more flexibility in the analysis and design on dynamical systems and controller solutions.

[4]Where contour plots are shown, these are done via grid search. Optimised results are found via a multi-start constrained optimization approach (i.e. a random multi-start using Matlab's *fmincon*() function with a neighborhood search on the selected best outcome). It was found that ten iterations, for the random multistart, were sufficient for the purposes of this work. A heuristics approach is an alternative approach that can also be used.

Figure 6 presents Bode plots for fractional integration, i.e. $1/s^{(1/n)}$ where $n \in \mathbb{R}$ (fractional integrators are also known as "tilted" integrators). The integration orders presented are: $n = 0.8, 1.2$ (with integrator gain crossover frequency at 1 rad/s). From a loop shape viewpoint the magnitude slope, $\frac{\mathrm{d}\log|G_i(j\omega)|}{d\log\omega}$ for $i = 0.8, 1.2$, at the gain crossover frequency is -0.8 and -1.2 (compared to a conventional integrator $1/s$ having slope of -1). Their phase contribution is $-72\,\mathrm{deg}$ and $-108\,\mathrm{deg}$ (compared to $1/s$ contributing $-90\,\mathrm{deg}$) respectively.

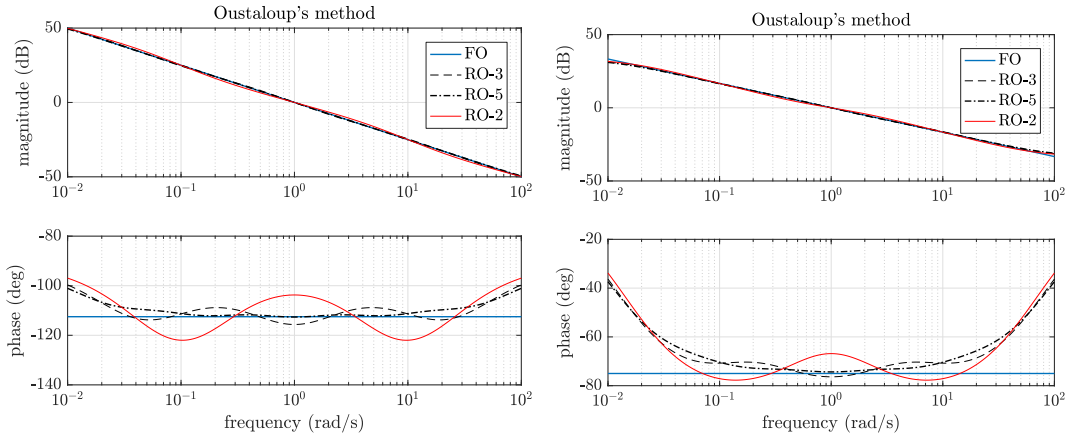

(a) For $1/s^{1.2}$ (b) For $1/s^{0.8}$

Figure 6. Fractional order integration and rational approximation examples (Bode plot)

The rational order (RO) approximation of the fractional order element is done via *Oustaloup's recursive method* [28], which is a popular approach in the fractional order control community (basic information on this is presented in Appendix B). Figure 6 illustrates rational order approximation by different orders Oustaloup approximation, in the frequency range of $[10^{-2},\ 10^{2}]$ rad/s. The concept is the same if approximation is required within different frequency regions. Note that rational approximations can also be obtained via frequency domain identification tools as an alternative.

6. Fractional order skyhook damping formulation

6.1. *Introducing fractional control to pure skyhook damping*

Here the tilted integrator is introduced to the skyhook damping scheme, see Figure 7 (but with no HP filter). The fractional integrator transfer function is $I_t(s) := \left(\frac{1}{s}\right)^{1/n}$ (ω_{tig} the integrator gain crossover frequency is shown as unity). The frequency region employed for approximation of all fractional order controllers in this work is actually $\{0.01, 100\}$ rad/s (as it offers sufficient detail for the designs involved). From a pure skyhook point of view the above is mapped as feeding back either a deficient or an excess order of absolute body velocity. Referring to (2) and Figure 2 (without considering the HP filter), the loop transfer function for the ideal case with tilted integrator, and assuming no HP

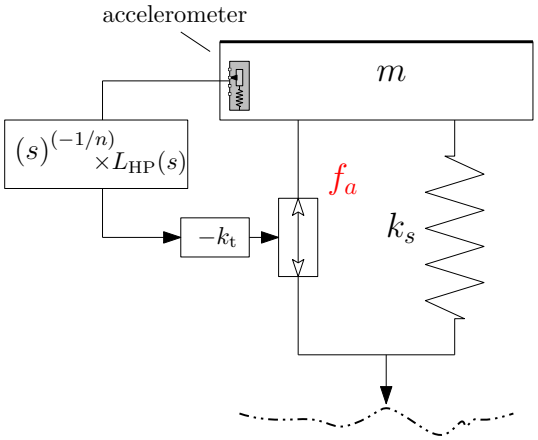

Figure 7. Practical skyhook damping scheme with fractional order (tilted) integrator

filter dynamics, is

$$L(s) = s^{(-1/n)}G(s)k_t = s^{(-1/n)}\,\frac{k_t s^2}{ms^2 + k_s} \tag{10}$$

Given that $(j\omega)^\nu$ can be represented by

$$(j\omega)^\nu = \omega^\nu e^{\frac{j\nu\pi}{2}} = \omega^\nu \left[\cos\left(\frac{\nu\pi}{2}\right) + j\sin\left(\frac{\nu\pi}{2}\right)\right] \tag{11}$$

where $j = \sqrt{-1}$, the magnitude and phase of $L(j\omega)$ are

$$|L(j\omega)| = \frac{\omega^{[2-(1/n)]}k_t}{-k_{\mathrm{s}} + m\omega^2} \tag{12}$$

$$\angle L(j\omega) = \begin{cases} \pi\left(1 - \frac{1}{2n}\right)\,, & \omega < \sqrt{\frac{k_{\mathrm{s}}}{m}} \\ -\frac{\pi}{2n}\,, & \omega > \sqrt{\frac{k_{\mathrm{s}}}{m}} \end{cases} \tag{13}$$

and the above could be used to design analytical compensated FO gain and phase margins if needed. Then, the resulting closed-loop referring to Figure 2 (taking into account fractional order conditions)

$$T_{\dot{z}^*_{\mathrm{m}} \leftarrow \dot{z}^*_{\mathrm{ref}}}(s) = \frac{s^{(2-n^{-1})}k_{\mathrm{t}}}{k_{\mathrm{t}}s^{(2-n^{-1})} + ms^2 + k_{\mathrm{s}}} \tag{14}$$

It is rather straightforward to obtain the closed-loop relationship from track velocity input to suspension deflection output for the above case, i.e.

$$\frac{(z_r - z_m)}{\dot{z}_r}(s) = \frac{k_{\mathrm{t}}\, s^{(1-n^{-1})} + m\, s}{k_{\mathrm{t}}\, s^{(2-n^{-1})} + m\, s^2 + k_{\mathrm{s}}} \tag{15}$$

Note that for $n = 1$, and $k_t := c_{\mathrm{t}}$, the expression coincides with the one from the basic *pCsky* scheme. Figure 8 illustrates the effect on suspension deflection response by varying the fractional order n (the variables are varied manually in this case).

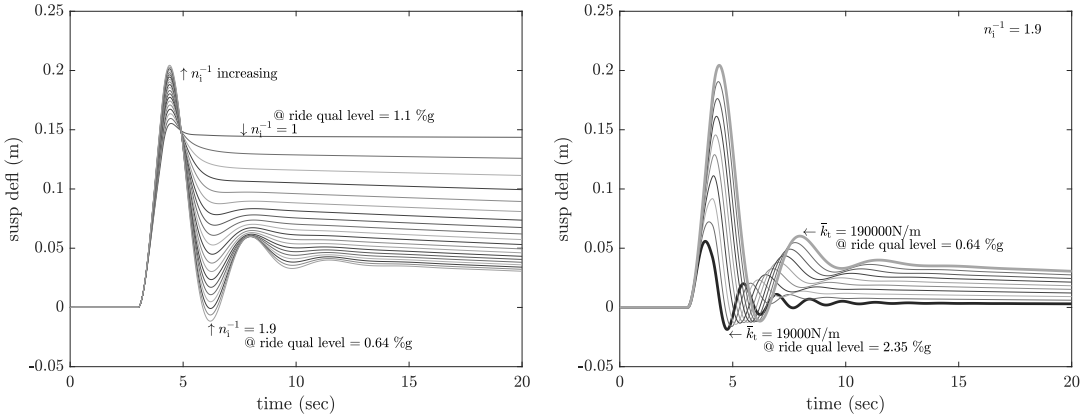

(a) $\bar{k}_t = 190000$ N/m ($\omega_{tig} = 1$ rad/s), n varies

(b) ω_{tig} varies (i.e. $\bar{k}_t$), $n^{-1} = 1.9$

Figure 8. Effect of fractional integration on *pCsky* (fractional system simulation)

For fine tuning the fractional order related optimization problem (19) (without considering the variables linked to the High-Pass filter but tuning n and the controller gain via ω_{tig}) is followed, and the obtained optimised values are

$$n^{opt} = 1.14, \quad k_t^{opt} = 42286.7 \text{ N/m} \tag{16}$$

Note that we again follow tuning the (now) fractional integrator gain crossover frequency

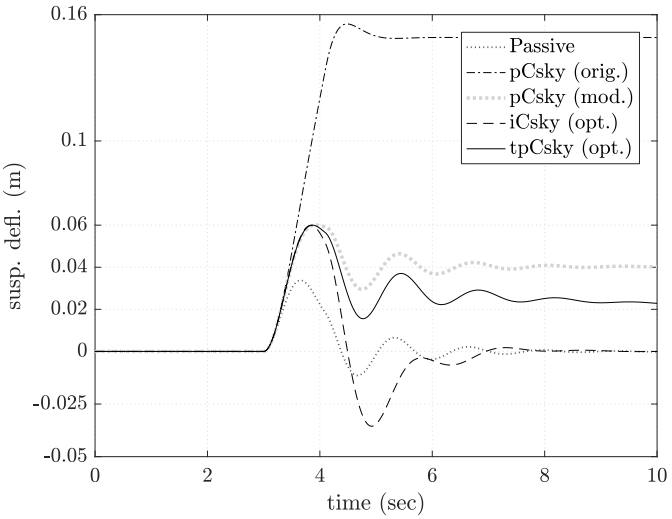

Figure 9. Suspension deflection response for *tpCsky* vs conv. skyhook schemes

ω_{tig} to maintain variables of comparable order in the optimization process (i.e. $k_t := \bar{k}_t \times \omega_{tig}^{(1/n)}$ is the final controller gain whereby $\bar{k}_t = 190$ kNs/m). Figure 9 presents the suspension deflection response (deterministic). The optimised values, to adhere to maximum suspension deflection of 60 mm, provide ride quality level of 2.11%g with imposed minimum closed-loop damping of $\approx$ 17%. The contour plot is presented on Figures 5(c), 5(d) for completeness. It is seen that the simplest extension using fractional

order integration on pure skyhook damping impacts the suspension deflection steady-state response, essentially offering a response "between" those of pure and practical skyhook damping schemes . Overall, the very simple fractional order scheme extension offers minor improvement to the trade-off (see Figure 10(a)), with its main impact on the steady-state response. But clearly it is a first indication that fractional order enables further design flexibility.

It is worth mentioning that, for the schemes with multiple variable tuning, Figure 10 presents the trend in the maximum suspension deflection / ride quality trade-off with the best ride quality chosen at each maximum suspension deflection point (to a 3 decimal point resolution). For a more proper and detailed view one should actually refer to surface plots (we present a couple of examples for later schemes).

For completeness, Table 2 presents the performance results for this scheme as well, and it is worth noting that typically robustness concerns are raised with $\|S_{cl}^{p}(j\omega)\|_{\infty} > 2$, whereas at a value of 2 the guaranteed gain margin is at least 2 (6 dB) and phase margin of at least 30deg (with this metric used as a basic robustness indicator).

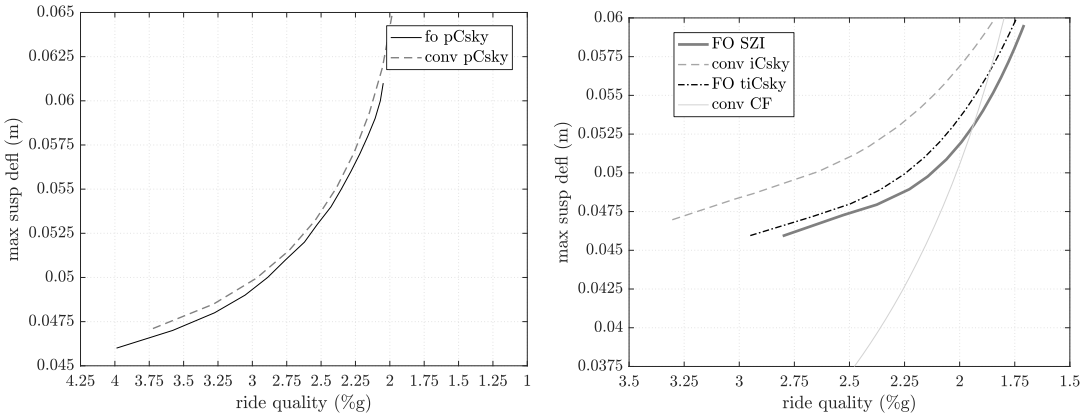

(a) Basic skyhook schemes

(b) Intuitively-based skyhook

Figure 10. Ride quality (rq)/ max susp deflection (msd) trend (best rq per msd)

6.2. *Extending to practical fractional order skyhook damping control*

The introduction of a HPF in the feedback structure has a direct effect on system order, which is illustrated in the transfer function relationship of track velocity input to suspension deflection output (see (17)). A 2nd order filter is still employed (for fair comparison to the conventional schemes).

$$\frac{z_r - z_m}{\dot{z}_r}(s) = \frac{\mathbf{k_t s^{(3-n^{-1})}} + ms^3 + 2\xi m\omega_{\rm fc}s^2 + m\omega_{\rm fc}^2 s}{\mathbf{k_t s^{(4-n^{-1})}} + ms^4 + 2\xi m\,\omega_{\rm fc}s^3 + (k_{\rm s} + \omega_{\rm fc}^2 m)\,s^2 + 2\xi k_{\rm s}\omega_{\rm fc}s + k_{\rm s}\omega_{\rm fc}^2} \quad (17)$$

[4]Recall the modified *pCsky* adheres to 60mm maximum suspension deflection and used only for illustration.

Table 3. Practical skyhook damping control schemes (conventional / fractional)

Scheme	**Info./ tuned vars**	ride qual. (%g)†	max susp. defl. (mm)	min{ζ} (%)	$\|\mathbf{S}^{\mathbf{p}}_{\mathbf{cl}}(\mathbf{j}\omega)\|_\infty$ (abs)
iCsky$^{(man.)}$ [conv.]	$\omega_{\rm fc}$	1.270	89.0	23.9	2.22
iCsky$^{(optim.\text{-}A)}$ [conv.]	$\omega_{\rm fc}, c_{\rm t}$	1.843	60.0	26.9	1.40
iCsky$^{(optim.\text{-}B)}$ [conv.]	$\omega_{\rm fc}, \xi, c_{\rm t}$	1.808	60.0	31.4	1.52
tiCsky [fractional]	♯	1.733	60.0	24.3	1.65
tifCsky [fractional]	§	1.706	60.0	25.6	1.84

† Single-sided spectrum; ♯ 2nd order HP filter, tuning $\omega_{\rm fc}, n, \xi$ in the optimization.
§ Overall fractional order "self zero integrator" (see (20)), tuning $\omega_{\rm fc}, \xi, n$, in the optimization.

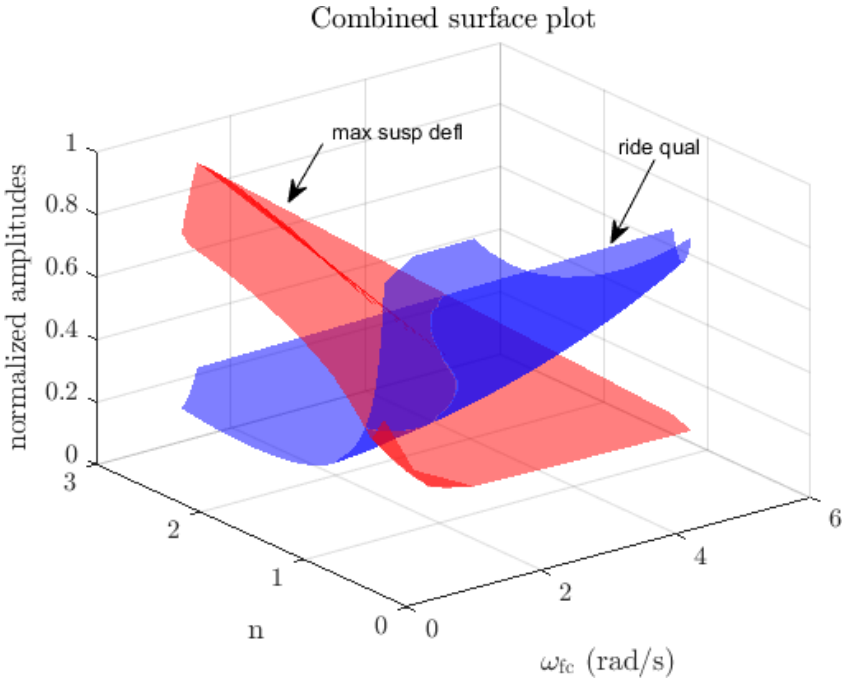

Figure 11. Surface plot for *tiCsky* (optim.)

which reduces to the equivalent TF in *iCsky*, if $k_{\rm t} := c_{\rm t}$ Ns/m and $n = 1$, i.e.

$$\left.\frac{z_r - z_m}{\dot{z}_r}(s)\right|_{\substack{n\ =1\\ k_{\rm t}\ =c_{\rm t}}} = \frac{ms^3 + (2\xi m\omega_{\rm fc} + \mathbf{c_t})\mathbf{s^2} + m\omega_{\rm fc}^2 s}{ms^4 + (2\xi m\omega_{\rm fc} + \mathbf{c_t})\mathbf{s^3} + (k_{\rm s} + \omega_{\rm fc}^2 m)\, s^2 + 2\xi k_{\rm s}\omega_{\rm fc} s + k_{\rm s}\omega_{\rm fc}^2} \tag{18}$$

$$\begin{aligned} \text{optimisation problem:}\quad & \underset{n,\omega_{\rm fc},\xi\ \in\mathbb{R}_+}{\text{minimize}} && \{\text{ride quality (active fo)}\} \\ & \text{subject to} && \max\{|z_r - z_m|\} \leq \quad 60\text{mm} \end{aligned} \tag{19}$$

In (19), $n^{-1}, \omega_{\rm fc}, \xi$ are the fractional order of the integrator, the HP filter cut-off frequency, and the damping ratio for the HP filter (where required).

First a simple optimization is followed (based on (19)), i.e. by tuning the fractional

order of the integrator and the (integer 2nd order) HP filter cut-off frequency and damping ratio, whereas the controller gain is fixed at 190 kNs/m. This represents a simple extension to fractional order practical skyhook damping scheme (this optimization case also serves are a fair or direct comparison with the conventional practical skyhook presented in [4] where only the HP filter cut-off frequency was tuned). The optimised values for the fractional order scheme obtained are: for the HP integer-order filter $\omega_{\rm fc}^{\rm opt} = 2.88$ rad/s, $\xi^{\rm opt} = 0.552$ and fractional order of integrator $n^{\rm opt} = 0.69$ (and it is interesting to see that the process provides integration effort above first order integration i.e. $1/n^{\rm opt} \approx 1.45$). For completeness, we present the combined surface plot for ride quality and maximum suspension deflection on Figure 11[5] (the trade-off is clearly seen). The trend is also mapped onto a 2-D plot on Figure 10(b) (the best ride quality at each maximum suspension deflection point selected) which illustrates the benefit of fractional order control (also see Table 3).

Next we directly consider a fractional order "self-zero" integrator, (here we present one with a 2nd order HP filter basis) i.e.

$$H_{\rm fsz2}(s) := (L_{\rm i}(s)L_{\rm HP}(s))^{1/n} = \left(\frac{s}{s^2 + 2\xi\omega_{\rm fc} + \omega_{\rm fc}^2}\right)^{1/n} \tag{20}$$

The importance in using the fractional order self zero integrator is that the fractional order reflects to the combined effort of integrator and HP filter (a.k.a. self-zero integration). Using a 2nd order HP filter (20) provides the opportunity of (refine) tuning the filter damping (although it is seen that the procedure results to a damping factor within 12% different to the typical value of 0.707 chosen manually [4], [24],[25]). This scheme is implemented by the feedback structure shown in Figure 12.

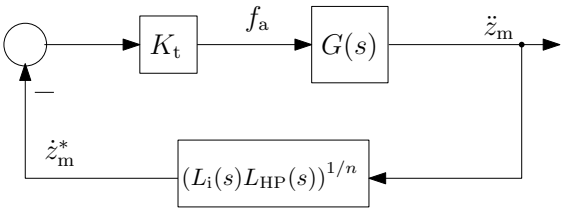

Figure 12. Skyhook feedback control scheme with FO "self-zero" integrator (*tifCsky*)

We present the optimized result for case *tifCsky*. A search bound between 0.55 and 0.875 was used for the HPF damping ratio. The optimised values (referring to optimization problem (19)) obtained were: $\omega_{\rm fc}^{\rm opt} = 2.02$ rad/s, $n^{\rm opt} = 0.71$, $\xi^{\rm opt} = 0.62$.

Note that in the optimization process no minimum closed-loop damping constraint is imposed. The performance results are also summarised in Table 3.

We also illustrate surface plots (maximum suspension deflection and ride quality)for *tifCsky* on Figure 13[6]. Due to the three variables in the optimization process, the plots are presented in the form of ternary diagram [29], with the axes representing normalized variables. The plots are shown to illustrate the trade-off relationship between suspension deflection and ride quality (clearly seen on the interchange of color shading in the plots). For further details on ternary diagrams the interested reader can refer to [29]. From the surface plots the presence of multiple local minima is also evident, hence the multi-start optimization approach used in the paper.

[5]As this is a combined surface plot, both ride quality and maximum suspension deflection are normalised relative

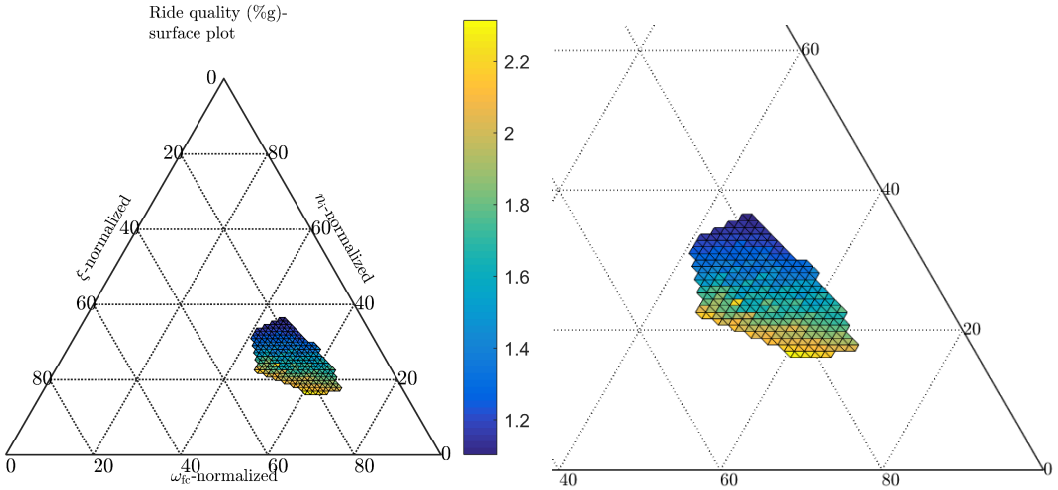

(a) Ride quality

(b) Ride quality (zoomed region)

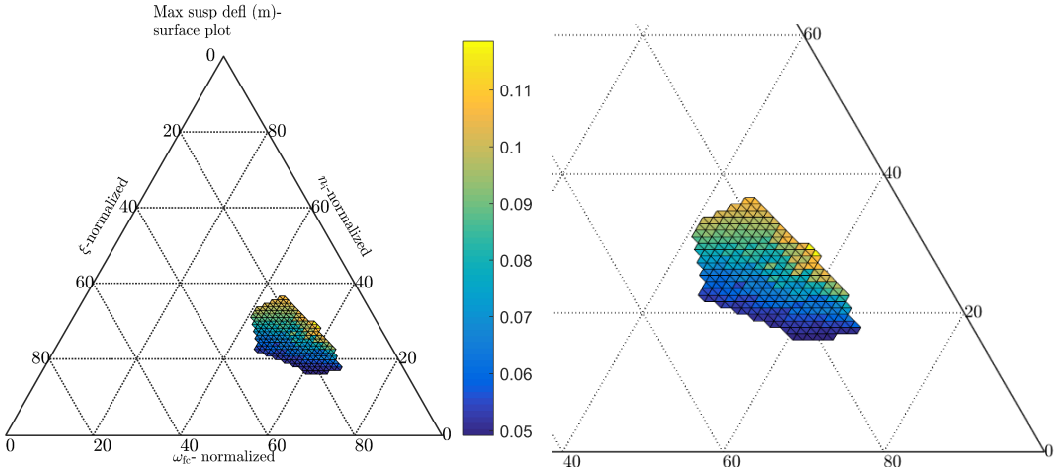

(c) Max susp defl

(d) Max susp. defl. (zoomed region)

Figure 13. Ternary diagram surface plots for *tifCsky*

From a (basic) robustness viewpoint all fractional order schemes manage to maintain a sensitivity peak value below 2, even if this constraint was not explicitly included in the optimization process. In fact the worst case is 1.84 which typically refers to a gain margin of at least 2.2 (6.85 dB) and a phase margin of at least 32 deg.

For completeness, the magnitude plot of the closed-loop system for ride quality is presented in Figure 14 for the designs with results presented in the previous performance tables (the cases listed are the *iCsky* (optim.-B), *tiCsky* and *tifCsky*). The improvement of system performance offered by the fractional order schemes is clearly evident in this plot as well. The time domain simulation for suspension deflection is shown on Figure 14(b).

Remark on comparisons to Complementary filter. We have presented an overall

to their maximum value.

[6]The unscaled variables range is: $\omega_{\rm fc} \in [1.25, 2.5]$ rad/s, $n_{\rm i} \in [0.6, 1.1]$, $\xi \in [0.55, 0.9]$ with only stable cases shown.

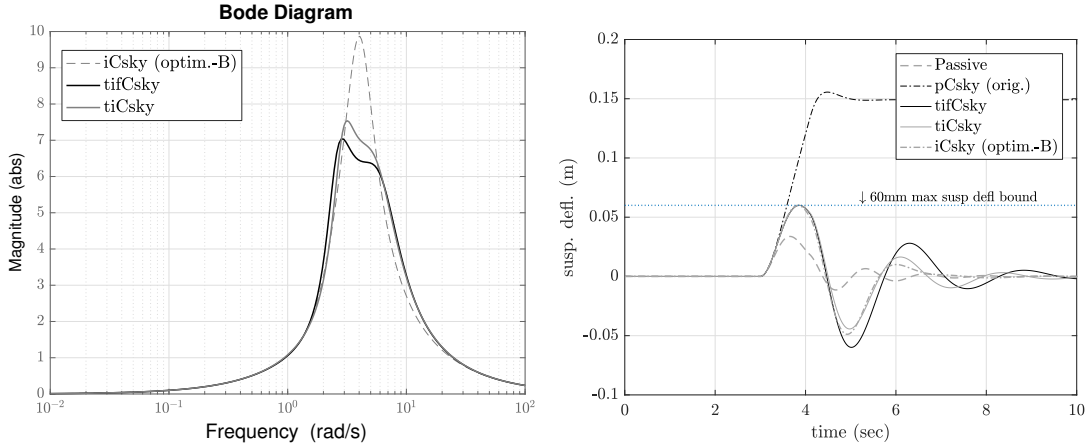

(a) Ride quality (bode plot)

(b) Suspension deflection (simulation)

Figure 14. Fractional order skyhook performance

performance trend mapped to the 2-D Figure 10. On Figure 10(b) a plot for the established conventional Complementary Filter approach (as proposed in [4]) is also shown. Note that we do not address complementary filter schemes in this paper, and the comparison is primarily to illustrate where the basic/practical fractional order schemes proposed here stand within the remit of skyhook control schemes. A note in the Conclusions section is also included regarding the nature of this paper.

7. Discussion on robustness for the practical skyhook schemes

We present a first look at the robustness of the schemes, mainly stemming from the results presented via the peak of the designed closed-loop sensitivity to plant variations. Note that robustness was not directly tackled in the optimization problem but, intentionally, explored the natural outcome of the process (i.e. referring to the sensitivity peak in the relevant performance Tables). The uncertainty considered is 100 perturbed plant cases based on the combination of vehicle mass uncertainty and stiffness uncertainty ($\pm 20\%$ parameter variation from their nominal values; note the absence of passive damping as in the nominal case). Figure 15(a) presents the Bode plot of the perturbed plant cases (with nominal plant highlighted).

The controllers for all cases are the ones design on the nominal model per scheme. Out of the 101 (100 perturbations and the nominal case) plant cases, the following maintain maximum suspension deflection below 60mm (in the closed-loop): 52 for *tifCsky*, 40 for *tiCsky*, 48 for *iCsky* (optim.-B), and 51 for *iCsky* (optim.-A). In addition, and from a statistical robustness point of view via the box-and-whisker plots on Figure 15, one can see a rather consistent interquartile range in all cases for ride quality, Figure 15(c), however the fractional order schemes offer smaller values of ride quality (under variation). The maximum suspension deflection case is more "balanced" (Figure 15(b)) in terms of the range of values, with the most schemes being balanced around 60mm (although *tiCsky* has drifted a little higher) and the interquartile range trend tends to narrow down as one moves from *tifCsky* to *tiCsky*, *iCsky* (optim.-B) and *iCsky* (optim.-A). The sensitivity peak metric is a "deterministic" robustness metric, and given that the "best" sensitivity peak value related to *iCsky* (optim.-A), what is shown in the latter

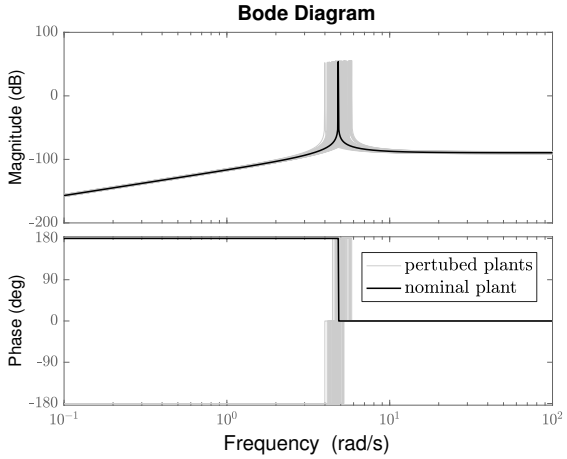

(a) Design plant uncertainty

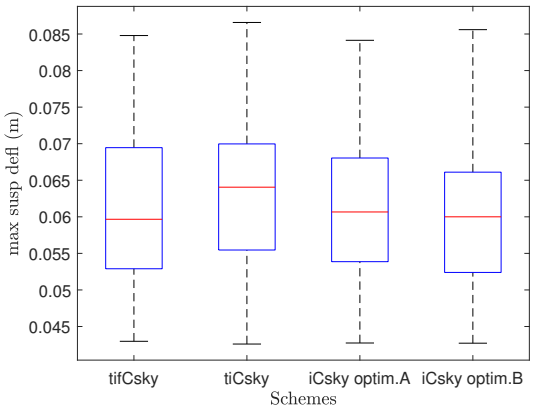

(b) Max suspension deflection (boxplot)

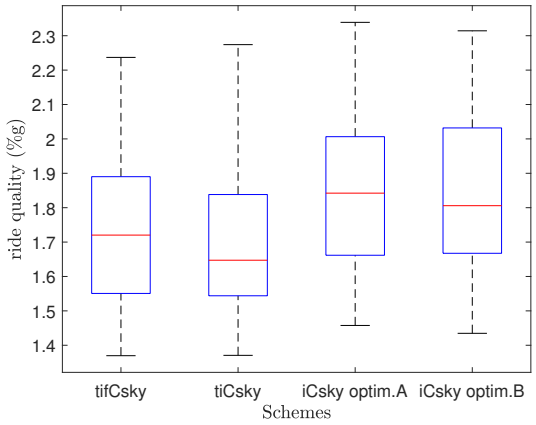

(c) Ride quality (boxplot)

Figure 15. Plant uncertainty and statistical robustness of practical skyhook schemes

plot is rather consistent with the indication on robustness level per scheme shown on the relevant performance tables. Clearly, the fractional order schemes offered better ride quality performance (for the same maximum suspension deflection levels) and maintained comparable robustness to the conventional schemes.

8. Conclusions

A rigorous study on the impact of fractional order methods in the design of basic and practical active secondary skyhook-type suspensions was presented. In particular the trade-off between ride quality and suspension deflection offered by the fractional order schemes have been considered and rigorously compared to established conventional integer order controller approaches [4] (from which this work was partly motivated). It is shown that fractional order methods offer an additional degree-of- freedom in the design process, and the basic principles examined in this work to provide a first insight at the opportunities. The authors believe that fractional order methods will steadily find their way into railway control applications. In fact, this paper represents a starting

point for further study encompassing a wider range of control options. The study has clearly identified the noticeable benefits in fractional order skyhook, typically offering 10-20% improvement in ride quality with the same maximum suspension deflection. The following specific comments are highlighted for the proposed fractional order schemes:

(i) It is a linear-time invariant solution (see rational approximation) based on a single measurement (feedback of acceleration utilised);
(ii) The pure integrator is essentially transformed (via its rational approximation version and depending on its order) towards an extended "PID-type" controller;
(iii) Performance wise, fractional order skyhook schemes noticeably surpass the performance of equivalent conventional skyhook schemes, while it is comparable to the conventional complementary filter performance down to about 52.5m max susp deflection level (for the case studied here).

Optimization tools were used extensively for the fractional order schemes, due to the extra design parameters. Similar optimization approach has been followed for the conventional controllers mainly for fair comparison between the two types of control schemes. In addition, the paper presents some initial assessment of robustness. The authors are currently extending the work via incorporation of advanced filtering schemes and detailed robustness investigation, for further appraisal of conventional vs. fractional-order methods in the aforementioned topic.

References

[1] Goodall R. Active railway suspensions: Implementation status and technological trends. Vehicle System Dynamics. 1997;28(2-3):87–117.
[2] Bruni S, Goodall R, Mei T, Tsunashima H. Control and monitoring for railway vehicle dynamics. Vehicle System Dynamics. 2007;45(7-8):743–779.
[3] Karnopp D. Are active suspension really necessary? ASME Paper, WA/DE-12; 1978. Report No.: 78.
[4] Li H, Goodall RM. Linear and non-linear skyhook damping control laws for active railway suspensions. Control Engineering Practice. 1999;7(7):843 – 850; Available from: http://www.sciencedirect.com/science/article/pii/S0967066199000489.
[5] Tavazoei MS. Time response analysis of fractional-order control systems: A survey on recent results. Fractional Calculus and Applied Analysis. 2014;17(2):440–461.
[6] Monje CA, Vinagre BM, Feliu V, Chen Y. Tuning and auto-tuning of fractional order controllers for industry applications. Control Engineering Practice. 2008;16(7):798 – 812; Available from: http://www.sciencedirect.com/science/article/pii/S0967066107001566.
[7] Bohannan GW. Analog fractional order controller in temperature and motor control applications. Journal of Vibration and Control. 2008;14(9-10):1487–1498.
[8] Petráš I, Vinagre B. Practical application of digital fractional-order controller to temperature control. Acta Montanistica Slovaca. 2002;7(2):131–137.
[9] Gonzalez E, Dorčák L, Monje C, Valsa J, Caluyo F, Petráš I. Conceptual design of a selectable fractional-order differentiator for industrial applications. Fractional Calculus and Applied Analysis. 2014;17(3):697–716.
[10] Caponetto R, Graziani S, Tomasello V, Pisano A. Identification and fractional super-twisting robust control of ipmc actuators. Fractional Calculus and Applied Analysis. 2015;18(6):1358–1378.
[11] Aldair AA, Wang WJ. Design of fractional order controller based on evolutionary algorithm for a full vehicle nonlinear active suspension systems. Int'l Journal of Control and Automation. 2010; 3(4):33–46.
[12] Chen N, Chen N, Tai Y. A numerical scheme for nonlinear dynamic system with fractional feedback control. In: 7th European Nonlinear Oscillations Conference; Jul; 2011.
[13] Dong X, Zhao D, Yang B, Han C. Fractional-order control of active suspension actuator based on parallel adaptive clonal selection algorithm. Journal of Mechanical Science and Technology. 2016; 30(6):2769–2781; Available from: http://dx.doi.org/10.1007/s12206-016-0538-2.

[14] Lanusse P, Poinot T, Cois O, Oustaloup A, Trigeassou J. Tuning of an active suspension system using a fractional controller and a closed-loop tuning. In: 11th international conference on advanced robotics; 2003. p. 258–263.
[15] Moreau X, Rizzo A, Oustaloup A. Application of the crone control-design method to a low-frequency active suspension system. Int'l Journal of Vehicle Autonomous Systems. 2009;7(3-4):172–200.
[16] Gad S, Metered H, Bassuiny A, Ghany AA. Multi-objective genetic algorithm fractional-order pid controller for semi-active magnetorheologically damped seat suspension. Journal of Vibration and Control. 2017;23(8):1248–1266; Available from: http://dx.doi.org/10.1177/1077546315591620.
[17] Baig WM, Hou Z, Ijaz S. Fractional order controller design for a semi-active suspension system using nelder-mead optimization. In: 2017 29th Chinese Control And Decision Conference (CCDC); May; 2017. p. 2808–2813.
[18] Zamani AA, Tavakoli S, Etedali S. Fractional order pid control design for semi-active control of smart base-isolated structures: A multi-objective cuckoo search approach. ISA transactions. 2017; 67:222–232.
[19] Tseng HE, Hrovat D. State of the art survey: active and semi-active suspension control. Vehicle System Dynamics. 2015;53(7):1034–1062; Available from: http://dx.doi.org/10.1080/00423114.2015.1037313.
[20] Tenreiro Machado J, Kiryakova V, Mainardi F. A poster about the old history of fractional calculus. Fractional Calculus and Applied Analysis. 2010;13(4):447–454.
[21] Hassan F, Zolotas A, Margetts R. Improved pid control for tilting trains. In: 2016 International Conference for Students on Applied Engineering (ICSAE); Oct; 2016. p. 269–274.
[22] Hassan F, Zolotas A. Impact of fractional order methods on optimized tilt control for rail vehicles. Fractional Calculus & Applied Analysis. 2017 Jun;20(3):765–789.
[23] Goodall R. Performance limitations for active secondary railway suspensions. In: Proceedings of the JSME conference STECH; Vol. 93; 1993. p. 81.
[24] Williams RA. Automotive active suspensions part 1: Basic principles. Proceedings of the Institution of Mechanical Engineers, Part D: Journal of Automobile Engineering. 1997;211(6):415–426; Available from: http://dx.doi.org/10.1243/0954407971526551.
[25] Williams RA. Automotive active suspensions part 2: Practical considerations. Proceedings of the Institution of Mechanical Engineers, Part D: Journal of Automobile Engineering. 1997;211(6):427–444; Available from: http://dx.doi.org/10.1243/0954407971526560.
[26] Skogestad S, Postlethwaite I. Multivariable feedback control: analysis and design. Vol. 2. Wiley New York; 2007.
[27] Podlubny I. Fractional differential equations: an introduction to fractional derivatives, fractional differential equations, to methods of their solution and some of their applications. Vol. 198. Academic press; 1998.
[28] Vinagre B, Podlubny I, Hernandez A, Feliu V. Some approximations of fractional order operators used in control theory and applications. Fractional calculus and applied analysis. 2000;3(3):231–248.
[29] Pawlowsky-Glahn V, Egozcue JJ. Compositional data and their analysis: an introduction. Geological Society, London, Special Publications. 2006;264(1):1–10.
[30] Petras I. Stability of fractional-order systems with rational orders. arXiv preprint arXiv:08114102. 2008;.
[31] Radwan AG, Soliman A, Elwakil AS, Sedeek A. On the stability of linear systems with fractional-order elements. Chaos, Solitons & Fractals. 2009;40(5):2317–2328.

Appendix A. Conventional rational order Skyhook stability

The high-pass filter used is a second (integer-)order filter (ξ the damping ratio), i.e.

$$L_{\mathrm{HP}}(s) = \frac{(s/\omega_{\mathrm{fc}})^2}{1 + 2\xi(s/\omega_{\mathrm{fc}}) + (s/\omega_{\mathrm{fc}})^2} = \frac{s^2}{\omega_{\mathrm{fc}}^2 + 2\xi\omega_{\mathrm{fc}}s + s^2} \tag{A1}$$

the Routh array for the CL system is:

$$\begin{array}{lccc} s^4\text{:} & 1 & \frac{m\,w_{\rm fc}^2+k_{\rm s}}{m} & \frac{k_{\rm s}\,w_{\rm fc}^2}{m} \\ s^3\text{:} & \frac{c_{\rm t}+2\,m\,\xi\,w_{\rm fc}}{m} & \frac{2\,k_{\rm s}\,\xi\,w_{\rm fc}}{m} & 0 \\ s^2\text{:} & \frac{2\,\xi\,m^2\,w_{\rm fc}^3+c_{\rm t}\,m\,w_{\rm fc}^2+c_{\rm t}\,k_{\rm s}}{m\,(c_{\rm t}+2\,m\,\xi\,w_{\rm fc})} & \frac{k_{\rm s}\,w_{\rm fc}^2}{m} & 0 \\ s^1\text{:} & -\frac{c_{\rm t}\,k_{\rm s}\,w_{\rm fc}\,(2\,m\,\xi\,w_{\rm fc}^2+c_{\rm t}\,w_{\rm fc}-2\,k_{\rm s}\,\xi)}{m\,(2\,\xi\,m^2\,w_{\rm fc}^3+c_{\rm t}\,m\,w_{\rm fc}^2+c_{\rm t}\,k_{\rm s})} & 0 & 0 \\ s^0\text{:} & \frac{k_{\rm s}\,w_{\rm fc}^2}{m} & 0 & 0 \end{array} \tag{A2}$$

Appendix B. Rational order approximation of fractional system

The interested reader can find more details on fractional order system rational approximations in [28]. Here only the very basic information for *Oustaloup's recursive method* is presented. For $D(s) := s^{\mu}, \quad \mu \in \mathbb{R}^+$ its rational order approximation using Oustaloup's method is given by

$$\widehat{D}(s) = C \prod_{k=-M}^{M} \frac{1+s/\omega_k}{1+s/\omega_k'}, \tag{B1}$$

where $C, M, \omega_k, \omega_k'$ are given by the theory of the approximation procedure (for details see [28]). The approximation is performed in a given frequency range, e.g. the rational approximation of $1/s^{1.14}$ (i.e. a single fractional integrator) by a 3rd order Oustaloup's approximant in the frequency range of $[10^{-2},\ 10^{2}]$ rad/s is given by

$$\hat{D}_{\rm ti}(s) = \frac{0.017604(s+0.1784)(s+3.844)(s+82.82)}{(s+0.01207)(s+0.2601)(s+5.605)}$$

clearly noting the approximate integrator in the denominator. The approach can be extended to more complex fractional order functions (approximation order increases with a higher number of integro-differential terms).

Appendix C. A note on fractional system stability

In the main body of the paper conventional, rational-order, system's stability and performance tools are employed (via the rational approximation of the FO controllers). Here, a brief note on fractional stability is presented. We refer to the *tpCsky* (no HP filter) (14). The denominator of the closed-loop, with the optimised values, is

$$\text{den}\{T_i(s)\} = 30000s^2 + 42287s^{1.1} + 700000 \tag{C1}$$

with the fractional power of s being appropriately truncated to 1 decimal point[7]. System designs presented in this paper involve both fractional and rational orders in the closed-

[7](For the purpose of this work 1 decimal point is sufficient, however note that finer decimal point resolution may shape the representation of fractional orders in forms of quotient of two integer numbers slightly different.)

loop, hence the fractional order stability test of [30], [31] is used.

In brief, the characteristic equation of the LTI system in s is transformed to the w-domain by an appropriate mapping $s = w^{\nu}$ (ν is integer); the roots of the transformed characteristic equation in the $w-$domain are calculated and their absolute phase is obtained, e.g. $|\phi_w|$; then (for the physical region $|\phi_w| < \pi/\nu$) the stability condition for the fractional system is

$$\frac{\pi}{2\nu} < |\phi_w| < \frac{\pi}{\nu} \tag{C2}$$

In our case, the characteristic equation (C1) can be translated to the $w-$domain by setting $w = s^{\frac{1}{10}}$, i.e. $0.043w^{20} + 0.06w^{11} + 1 = 0$. Figure C1 presents the stability results for the aforementioned FO closed-loop and it can be seen that $\frac{\pi}{20} < |\phi_w| < \frac{\pi}{10}$, hence the fractional order closed-loop is stable (Figure C1(b)). Note that the roots in the

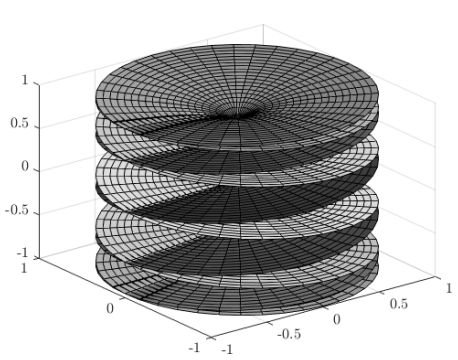

(a) Riemann surface of $w = s^{\frac{1}{10}}$ (10-sheets)

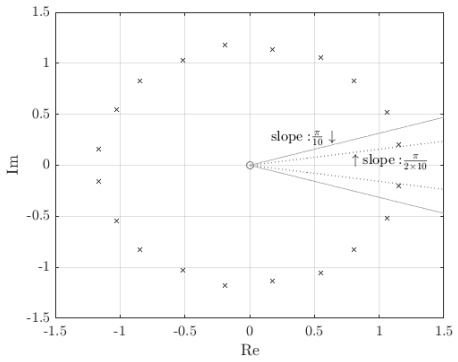

(b) Poles location in $w-$plane (fractional)

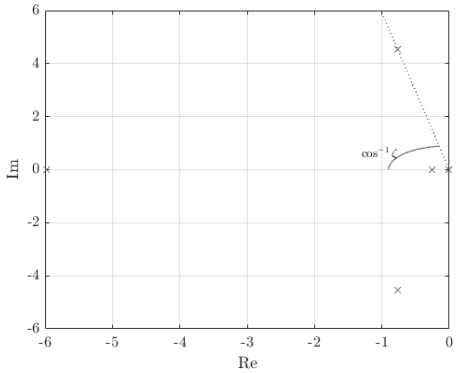

(c) Poles location in $s-$plane (rational)

Figure C1. Stability of *tpCsky* (fractional and rational approximation)

first Riemann sheet are $w_{19,20} = 1.149 \pm 0.202j$ with $|\arg(w_{19,20})| = 0.174$ satisfying the above condition. For completeness, Figure C1(c) presents the conventional stability result of the CL including the iso-damping line of minimum CL damping of 0.167.

Word count: approximately 7300 words.